11

Dynamic Characterization of Ancient Masonry Structures

Annamaria Pau and Fabrizio Vestroni
Università di Roma La Sapienza
Italy

1. Introduction

The analysis of the dynamic response induced in a structure by ambient vibrations is important for two reasons. On the one hand, the environmental impact of vibrations is a common cause for concern in many cities throughout the world on account of both the consequences of such vibrations on buildings, especially those in structurally weak conditions, and on people in terms of annoyance. On the other hand, the measured data contain information on the dynamic characteristics of the structures, such as modal parameters (frequencies, damping ratios and mode shapes). Several techniques of experimental modal analysis are nowadays well established and make it possible to extract modal parameters from the measurements of the dynamical response. Books on this topic are by (Bendat & Piersol, 1980; Ewins, 2000; Juang, 1994; Maia & Silva, 1997; Van Overschee & De Moor, 1996). A knowledge of modal parameters is a basic step for updating a finite element model which not only replicates the real response (Friswell & Mottershead, 1995), but also enables to build damage identification procedures based on the variation of the structural response (Morassi & Vestroni, 2009; Vestroni & Capecchi, 1996). Furthermore, periodical repetition of the measurement process over time, together with observation of possible variation of modal parameters, forms the basis for a structural health monitoring procedure (Farrar et al., 2001). These issues are especially important for ancient buildings, marked by complex geometry, heterogeneous materials and in poor conditions, which are often very sensitive to deterioration.

Experimental modal analysis usually deals with frequency response functions (FRF) in the frequency domain or impulse response functions in the time domain and requires that the response to an assigned input is measured. In civil structures, the system should be excited with heavy shakers (De Sortis et al., 2005), which makes these tests expensive and often impracticable, especially in the case of very large structures. The measurement of the ambient vibration response, which is the response to an unknown input due to natural and human actions (for instance wind, microtremors, traffic), makes it possible to overcome the difficulties that often arise when artificial excitation is used. The drawbacks in this kind of measurements are that there is the need to deal with signals with small amplitude and, furthermore, the hypothesis that the spectrum of the forcing function is approximately flat in the frequency band where the modes are to be estimated, which can not be fully experimentally proved, must be accepted. Of the several ambient vibration modal identification techniques, three will be described in this chapter: peak picking from the power spectral densities (PP) (Bendat

& Piersol, 1980), singular value decomposition (SVD) (Brincker et al., 2001) and stochastic subspace identification (SSI) (Peeters, 2000; Van Overschee & De Moor, 1993; 1994; 1996). The mentioned techniques have been successfully used for the modal identification of numerous civil structures, such as bridges (Ren et al., 2004) or tall buildings (Brownjohn, 2003), but less frequently applied to historical structures and monuments (Gentile & Saisi, 2007; Pau & Vestroni, 2008; 2010). This chapter aims to describe their application to selected cases of historical masonry structures in Italy.

Of late, some of the most important monuments in Rome have been investigated because of the proximity of these structures to a new underground line that is at present under construction. These tests include the recording of the ambient vibration response. The Colosseum, the Basilica of Maxentius and the Trajan Column are some of the investigated monuments. The availability of such data enables a dynamic characterization and identification of modal parameters of the structures, which presents a challenging task in such large and geometrically complex monuments, built with heterogeneous materials. Parts of the results of these experimental tests are reported in the works by (Pau & Vestroni, 2008; 2010). Here, the case of the Trajan Column will be discussed in detail together with another application to a railway masonry bridge of the 19th century. For each of these cases, a comparison between experimental and numerical modal parameters is discussed, in the perspective of the evaluation and updating of the finite element models according to the measured behavior. This comparison may enable the identification of the possible causes of discrepancies between predicted and measured properties. In particular, the information obtained may relate to the current state of a structure: lower natural frequencies than those predicted by the finite element model may indicate deterioration in the stiffness of the structure and anomalous mode shapes may point to the independent motion of structural parts due to major cracks. In many cases, notwithstanding the severe simplifications, mainly regarding the material behavior introduced in the numerical modeling, the comparison between numerical and experimental frequencies and mode shapes provides sufficient agreement, after an adjustment of the mechanical characteristics to tune the two models. This adjustment has shown to have a significant mechanical meaning indicating the effective presence of cracks and discontinuities (Pau & Vestroni, 2010).

2. Ambient vibration modal identification techniques

Very often, when dealing with large engineering structures such as building or bridges, it is impractical to measure the response to an *ad hoc* and controlled artificial excitation for different reasons, such as costs concern or even the unwanted possibility of activating nonlinear phenomena.

Reasonable estimates of modal properties can be obtained from an output-only analysis of the ambient vibration response to the natural dynamic environment. This excitation, which is random in its nature, is due to various human and artificial sources, such as traffic, wind and microtremors. When dealing with output-only analysis of the vibration response, it is fundamental to cope with signals with small amplitude and contaminated by noise. Although the input is unknown, which prevents from measuring the proper FRF, a hypothesis that the spectrum of the forcing function is flat in the frequency band where the modes are to be estimated must be made, which can only be partially proved from experiments. This paragraph describes three techniques of modal identification, which are important for different reasons. The peak picking from the power spectral densities is a frequency domain based technique and is important for historical reasons, since it was one of

the first output-only modal identification techniques to be presented in the late '70s (Bendat & Piersol, 1980), and its simplicity. The singular value decomposition is an extension of the peak picking (Brincker et al., 2001). With respect to the peak picking, it enables to deal better with close frequencies and damped modes. Its advantage over other recent techniques consists mainly in its preserving the user's understanding of the data he is dealing with through a frequency approach. In the early '90s, the stochastic subspace identification, which is a time domain technique, was described in research papers (Van Overschee & De Moor, 1993; 1994) and in the fundamental book by (Van Overschee & De Moor, 1996). Today, the SSI is one of the most widespread techniques for output-only modal identification and is implemented not only in commercial softwares for data analysis (Artemis) but also in Matlab routines and freely available software (http://homes.esat.kuleuven.be/ smc/sysid/software/).

2.1 Peak picking

This method is very often used for its simplicity in analysing the ambient vibration response, when the input is unknown (Bendat & Piersol, 1980). The ambient vibration response of a structure cannot be predicted by deterministic models, within reasonable error. Each experiment produces a random time-history that represents only one physical realization of what might occur. In general, the response $x(t)$ of the structure to ambient excitation is recorded for a very long time, even for hours, which enables to cut the random process $x(t)$ into a collection of subregistrations $x_k(t)$ which describe the phenomenon. The Fourier Transforms of the kth subregistrations of two random processes $x_k(t)$ and $y_k(t)$ are respectively:

$$X_k(f,T) = \int_0^T x_k(t) \exp^{-i2\pi ft} \, \mathrm{d}t \tag{1}$$

$$Y_k(f,T) = \int_0^T y_k(t) \exp^{-i2\pi ft} \, \mathrm{d}t. \tag{2}$$

The auto (or power) spectral density (PSD) and cross-spectral density (CSD) and related coherence function between the two random processes are respectively:

$$S_{xx}(f) = \lim_{T\to\infty} \frac{1}{T} E[\mid X_k(f,T) \mid^2] \tag{3}$$

$$S_{xy}(f) = \lim_{T\to\infty} \frac{1}{T} E[X_k^*(f,T) Y_k(f,T)] \tag{4}$$

$$\gamma_{xy}(f) = \frac{\mid S_{xy}(f) \mid^2}{S_{xx}(f) S_{yy}(f)} \tag{5}$$

where the symbol $E[.]$ indicates an averaging operation over the index k and the asterisk denotes complex conjugate.

Let us now assume that $x(t)$ is the input and $y(t)$ is the output. The auto-spectral and cross-spectral density functions satisfy the important formulae:

$$S_{yy}(f) = |H_{xy}(f)|^2 S_{xx}(f) \quad S_{xy}(f) = H_{xy}(f) S_{xx}(f) \tag{6}$$

where $H_{xy}(f)$ is the frequency response function. The simple peak picking method is based on the fact that the autospectrum (6_1), at any response point, reaches a maximum either when the excitation spectrum peaks or the frequency response function peaks. To distinguish between

peaks that are due to vibration modes as opposed to those in the input spectrum, a couple of criteria can be used. The former concerns the fact that in a lightly damped structure, two points must oscillate in-phase or out-of-phase. Then, the cross spectrum (6_2) between the two responses provides this information, which can be used to distinguish whether the peaks are due to vibration modes or not. The second criterion uses the coherence function (5), which tends to peak at the natural frequencies, as the signal-to-noise ratio is maximised at these frequencies.

2.2 Singular value decomposition

The second method referred to also relies only on the response to ambient excitations (output only). The method is based on the singular value decomposition of the response spectral matrix (Brincker et al., 2001), exploiting the relationship:

$$\mathbf{S}yy\,(\omega) = \mathbf{H}^{*}\,(\omega)\,\mathbf{S}xx\,(\omega)\,\mathbf{H}^{T}\,(\omega) \tag{7}$$

where $\mathbf{S}xx(\omega)$ ($r \times r$, r number of inputs) and $\mathbf{S}yy(\omega)$ ($m \times m$, m number of measured responses) are the input and output power spectral density matrices, respectively, and $\mathbf{H}(\omega)$ is the frequency response function matrix $(m \times r)$. Supposing the inputs at the different points are completely uncorrelated and white noise, $\mathbf{S}xx$ is a constant diagonal matrix, independent of ω. Thus:

$$\mathbf{S}yy\,(\omega) = S\,\mathbf{H}\,(\omega)\,\mathbf{H}^{T}\,(\omega) \tag{8}$$

whose term jk can be written, by omitting the constant S, as:

$$Syy_{jk}\,(\omega) = \sum_{r=1}^{r}\left(\sum_{p=1}^{n}\frac{\phi_{jp}\phi_{rp}}{\bar{\lambda}_{p}^{2}-\omega^{2}}\right)\left(\sum_{q=1}^{n}\frac{\phi_{kq}\phi_{rq}}{\lambda_{q}^{2}-\omega^{2}}\right). \tag{9}$$

In the neighbourhood of the ith resonance, the previous equation can be approximated by:

$$Syy_{jk}\,(\omega) \cong \sum_{r=1}^{r}\frac{\phi_{ji}\phi_{ri}}{\bar{\lambda}_{i}^{2}-\omega^{2}}\frac{\phi_{ki}\phi_{ri}}{\lambda_{i}^{2}-\omega^{2}} = \frac{\phi_{ji}\phi_{ki}}{\left(\bar{\lambda}_{i}^{2}-\omega^{2}\right)\left(\lambda_{i}^{2}-\omega^{2}\right)}\sum_{r=1}^{r}\phi_{ri}^{2}. \tag{10}$$

By ignoring the constant $\sum_{r=1}^{r}\phi_{ri}^{2}$, Syy can thus be expressed as the product of the three matrices:

$$\mathbf{S}yy\,(\omega) = \mathbf{\Phi}\mathbf{\Lambda}_{i}\mathbf{\Phi}^{T} \tag{11}$$

which represents a singular value decomposition of the matrix $\mathbf{S}yy$, where:

$$\mathbf{\Lambda}_{i} = \begin{bmatrix} \frac{1}{\left(\lambda_{i}^{2}-\omega^{2}\right)\left(\bar{\lambda}_{i}^{2}-\omega^{2}\right)} & 0\ldots & 0 \\ 0 & 0\ldots & 0 \\ \vdots & \vdots & \vdots \\ 0 & 0\ldots & 0 \end{bmatrix}. \tag{12}$$

This is valid in the neighbourhood of every natural frequency of the system, that hence emerges as a peak of the first singular value. The first column of the matrix $\mathbf{\Phi}$ contains the first singular vector, which, in the neighborhood of the ith resonance, coincides with the ith eigenvector. This occurs at each resonance, when the prevailing contribution is given by the related mode. This procedure has recently had great diffusion mainly in *in situ* experimental tests and has also been implemented in commercial codes.

2.3 Stochastic subspace identification

The stochastic subspace identification belongs to the wide class of time domain methods. The continuous-time dynamics of a discrete or a discretized (in space) mechanical system in the state-space can be written as:

$$\dot{\mathbf{x}}(t) = \mathbf{A}_c \mathbf{x}(t) + \mathbf{B}_c \mathbf{f}(t) \tag{13}$$

which is a representation deriving from the control theory (Juang, 1994). In this relationship, $\mathbf{x}(t) = [\mathbf{u}(t)^T \ \dot{\mathbf{u}}(t)^T] \in \mathbb{R}^{2n}$ is the state vector of the process. This vector contains the $2n$ states of the system, where $\mathbf{u}(t)$ and $\dot{\mathbf{u}}(t)$ are respectively the displacement and velocity vectors and n is the number of degrees-of-freedom. $\mathbf{A}_c \in \mathbb{R}^{2n \times 2n}$ is the continuous-time state matrix, which is related to the classical matrices of mass $\mathbf{M}$, damping $\mathbf{C}_d$ and stiffness $\mathbf{K}$ by:

$$\mathbf{A}_c = \begin{bmatrix} \mathbf{0} & \mathbf{I} \\ -\mathbf{M}^{-1}\mathbf{K} & -\mathbf{M}^{-1}\mathbf{C}_d \end{bmatrix}, \tag{14}$$

$\mathbf{f}(t) \in \mathbb{R}^n$ is the load vector and $\mathbf{B}_c \in \mathbb{R}^{2n \times n}$ is the system control influence coefficient matrix:

$$\mathbf{B}_c = \begin{bmatrix} \mathbf{0} \\ \mathbf{M}^{-1} \end{bmatrix}. \tag{15}$$

In a vibration experiment, only a subset l of the responses at the n degrees-of-freedom can be measured. The vector of the measured outputs $\mathbf{y}(t) \in \mathbb{R}^l$ is written as: $\mathbf{y}(t) = \mathbf{C}_a \ddot{\mathbf{u}}(t) + \mathbf{C}_v \dot{\mathbf{u}}(t) + \mathbf{C}_u \mathbf{u}(t)$, where $\mathbf{C}_a$, $\mathbf{C}_v$ and $\mathbf{C}_u$ are output location matrices for accelerations, velocities and displacements respectively, which are matrices of zeros and ones made up to select the measured degrees of freedom. The vector $\mathbf{y}(t)$ can be written as:

$$\mathbf{y}(t) = \mathbf{C}_c \mathbf{x}(t) + \mathbf{D}_c \mathbf{f}(t) \tag{16}$$

where $\mathbf{C}_c \in \mathbb{R}^{l \times 2n}$ is the output matrix and $\mathbf{D}_c \in \mathbb{R}^{l \times n}$ is the direct transmission matrix:

$$\mathbf{C}_c = [\mathbf{C}_u - \mathbf{C}_a \mathbf{M}^{-1}\mathbf{K} \quad \mathbf{C}_v - \mathbf{C}_a \mathbf{M}^{-1}\mathbf{C}_u] \quad \text{and} \quad \mathbf{D}_c = \mathbf{C}_a \mathbf{M}^{-1}. \tag{17}$$

Then, in conclusion, the continuous-time state-space model can be written as:

$$\begin{cases} \dot{\mathbf{x}}(t) = \mathbf{A}_c \mathbf{x}(t) + \mathbf{B}_c \mathbf{f}(t) \\ \mathbf{y}(t) = \mathbf{C}_c \mathbf{x}(t) + \mathbf{D}_c \mathbf{f}(t) \end{cases}. \tag{18}$$

It can be shown that the eigenvalues $\mathbf{\Lambda}_c$ and eigenvectors $\mathbf{\Psi}$ of the continuous state-space matrix $\mathbf{A}_c$ which solve the eigenvalue problem $\mathbf{A}_c \mathbf{\Psi} = \mathbf{\Psi} \mathbf{\Lambda}_c$ contain the eigenvalues $\mathbf{\Lambda}$ and eigenvectors $\mathbf{\Theta}$ of the original second-order system:

$$\mathbf{\Lambda}_c = \begin{pmatrix} \mathbf{\Lambda} & \mathbf{0} \\ \mathbf{0} & \mathbf{\Lambda}^* \end{pmatrix}, \quad \mathbf{\Psi} = \begin{pmatrix} \mathbf{\Theta} & \mathbf{\Theta}^* \\ \mathbf{\Theta}\mathbf{\Lambda} & \mathbf{\Theta}^*\mathbf{\Lambda}^* \end{pmatrix}. \tag{19}$$

In practice, experimental data are discrete. Therefore, the model of equation (18) has to be converted to discrete time, in order to fit the models to measurements. The continuous-time equations are discretized and solved at all the discrete time instants $t_k = k\Delta t, k \in \mathbb{N}$, where Δt is the sampling period. Let us suppose to focus the analysis on time-invariant state-space models. These deterministic-stochastic systems, excited both by deterministic and random actions, are described by the following set of difference equations:

$$\begin{cases} \mathbf{x}_{k+1} = \mathbf{A}\mathbf{x}_k + \mathbf{B}\mathbf{f}_k + \mathbf{w}_k \\ \mathbf{y}_k = \mathbf{C}\mathbf{x}_k + \mathbf{D}\mathbf{f}_k + \mathbf{v}_k \end{cases} \tag{20}$$

The vector $\mathbf{x}_k \in \mathbb{R}^{2n}$ is defined as the state vector of the process at the discrete time instant k. This vector contains the numerical values of the $2n$ states of the system. When dealing with mechanical systems, the state vector is $\mathbf{x}_k = [\mathbf{u}_k^T \ \dot{\mathbf{u}}_k^T] \in \mathbb{R}^{2m}$, $\mathbf{f}_k \in \mathbb{R}^n$ and $\mathbf{y}_k \in \mathbb{R}^l$ are respectively the experimental measurements at time instant k of the n inputs and l outputs. $\mathbf{w}_k \in \mathbb{R}^{2n}$ and $\mathbf{v}_k \in \mathbb{R}^l$ are respectively process and measurement noise vectors, which are unmeasurable quantities. The former is due to model inaccuracies, the latter due to measurement inaccuracies. $\mathbf{A}$ is the discrete state matrix, $\mathbf{B}$ is the discrete input matrix, $\mathbf{C}$ is the discrete output matrix and $\mathbf{D}$ is the direct transmission matrix. They are related to their continuous-time counterparts by the relationships:

$$\begin{array}{ll} \mathbf{A} = e^{\mathbf{A}_c \Delta t} & \mathbf{B} = \left(\int_0^{\Delta t} e^{\mathbf{A}_c \tau} d\tau \right) \mathbf{B}_c = (\mathbf{A} - \mathbf{I}) \mathbf{A}_c^{-1} \mathbf{B}_c \\ \mathbf{C} = \mathbf{C}_c & \mathbf{D} = \mathbf{D}_c. \end{array} \tag{21}$$

These well-established relationships can be found in the literature (Juang, 1994). The hypothesis:

$$\mathrm{E}\left[\begin{pmatrix} \mathbf{w}_p \\ \mathbf{v}_p \end{pmatrix} \begin{pmatrix} \mathbf{w}_q^T & \mathbf{v}_q^T \end{pmatrix} \right] = \begin{pmatrix} \mathbf{Q} & \mathbf{S} \\ \mathbf{S}^T & \mathbf{R} \end{pmatrix} \delta_{pq} \geqq 0 \tag{22}$$

is further added, where $\mathrm{E}[.]$ indicates the expected value and δ_{pq} is the Kronecker delta. The matrices $\mathbf{Q} \in \mathbb{R}^{2n \times 2n}$, $\mathbf{S} \in \mathbb{R}^{2n \times l}$ and $\mathbf{R} \in \mathbb{R}^{l \times l}$ are the covariance matrices of the noise terms $\mathbf{w}_k$ and $\mathbf{v}_k$, which are supposed to be independent of each other and both with zero mean. It must be remarked that in output-only modal identification, the input sequence $\mathbf{f}_k$ is unmeasured and only the response $\mathbf{y}_k$ is known. Hence, it is impossible to distinguish the input term $\mathbf{f}_k$ from the noise terms $\mathbf{w}_k$ and $\mathbf{v}_k$ in equation (20). This results in a purely stochastic system:

$$\begin{cases} \mathbf{x}_{k+1} = \mathbf{A}\mathbf{x}_k + \mathbf{w}_k \\ \mathbf{y}_k = \mathbf{C}\mathbf{x}_k + \mathbf{v}_k \end{cases} . \tag{23}$$

In equation (23), the white noise assumption on the terms $\mathbf{w}_k$ and $\mathbf{v}_k$ cannot be omitted. If the input contains some dominant frequency components, they will not be separated from the eigenfrequencies of the system. The stochastic subspace identification then moves from equations (23) to estimate the state-space matrices $\mathbf{A}$ and $\mathbf{C}$ from the measured output $\mathbf{y}_k$, with $k = 1, 2, \ldots, N$ and $N \longrightarrow \infty$. The estimate of state-space matrices can be performed by different algorithms. In the applications, the procedure described in the work by (Van Overschee & De Moor, 1994) is used. In short, this procedure is based on selected theorems of linear algebra illustrated in (Van Overschee & De Moor, 1994; 1996), which demonstrate that the state space matrices can be calculated from the knowledge of the block Hankel matrix. This matrix is obtained by casting the finite dimensional output vector $\mathbf{y}_k$ into

the columns of a semi infinite $2i \times j$ matrix:

$$U_{0|2i-1} = \left(\begin{array}{ccccc} y_0 & y_1 & y_2 & \cdots & y_{j-1} \\ y_1 & y_2 & y_3 & \cdots & y_j \\ \cdots & \cdots & \cdots & \cdots & \cdots \\ y_{i-1} & y_i & y_{i+1} & \cdots & y_{i+j-2} \\ \hline y_i & y_{i+1} & y_{i+2} & \cdots & y_{i+j-1} \\ y_{i+1} & y_{i+2} & y_{i+3} & \cdots & y_{i+j} \\ \cdots & \cdots & \cdots & \cdots & \cdots \\ y_{2i-1} & y_{2i} & y_{2i+1} & \cdots & u_{2i+j-2} \end{array} \right) \tag{24}$$

where the horizontal line divides *past* inputs from *future* inputs. Once the matrix $\mathbf{A}$ is known, the natural frequencies and mode shapes can be evaluated. In fact, as shown in (Peeters, 2000), the eigenvalues $\mathbf{\Lambda}_d$ and eigenvectors of the discrete state-space matrix are related to their continuous counterparts by the relationships:

$$\mathbf{A} = e^{\mathbf{A}_c \Delta t} = e^{\mathbf{\Psi}\mathbf{\Lambda}_c\mathbf{\Psi}^{-1}\Delta t} = \mathbf{\Psi} e^{\mathbf{\Lambda}_c \Delta t}\mathbf{\Psi}^{-1} = \mathbf{\Psi}\mathbf{\Lambda}_d\mathbf{\Psi}^{-1}. \tag{25}$$

That is, the eigenvectors are the same for both systems, while the discrete eigenvalues μ_i are related to the continuous eigenvalues λ_i by:

$$\lambda_i = \frac{\ln(\mu_i)}{\Delta t}. \tag{26}$$

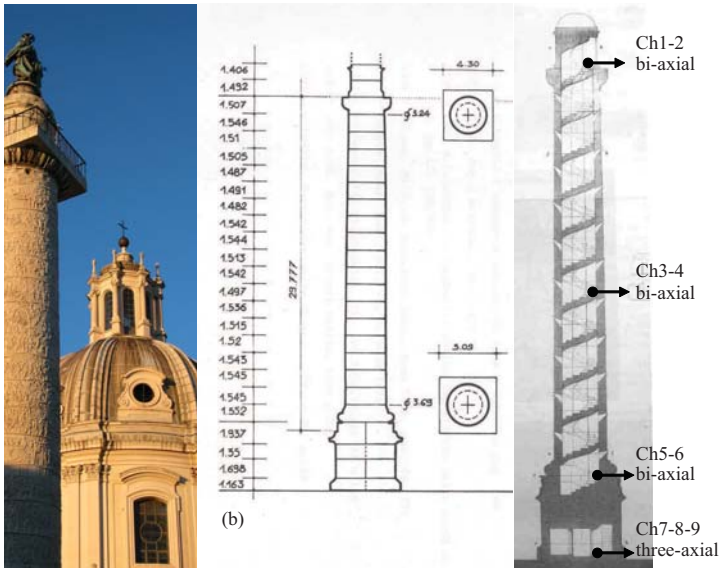

Fig. 1. A view of the Trajan column (a), its survey (b) and accelerometer setup (c).

3. Applications

3.1 The Trajan Column

The Trajan Column is a honorary monument that, in 113 A.D., was dedicated to Trajan the emperor to celebrate his triumph over the Dacians, the inhabitants of the present Romania. Over the surface of the column, a helical bas-relief depicts the story of Trajan's victory. The monument consists of a marble column about 30m tall, with a circular section having an external diameter of 3.55m, placed over a square-section pedestal 6.23m high (Figures 1 a-b). It represents a peculiarity in archaeological heritage because of its slenderness. The column is formed by nineteen cylindrical elements, dug-out to form an internal helical staircase going to the top level. The helical geometry is perturbed by tiny windows along the external surface. The response of this structure was measured by one three-axial set of accelerometers at the base and three biaxial horizontal sets at the upper levels. The measurement points with their related channels are reported in Figure 1c. The recordings were performed at a sampling frequency of $f_s = 300Hz$ for a duration of about 2 hours.

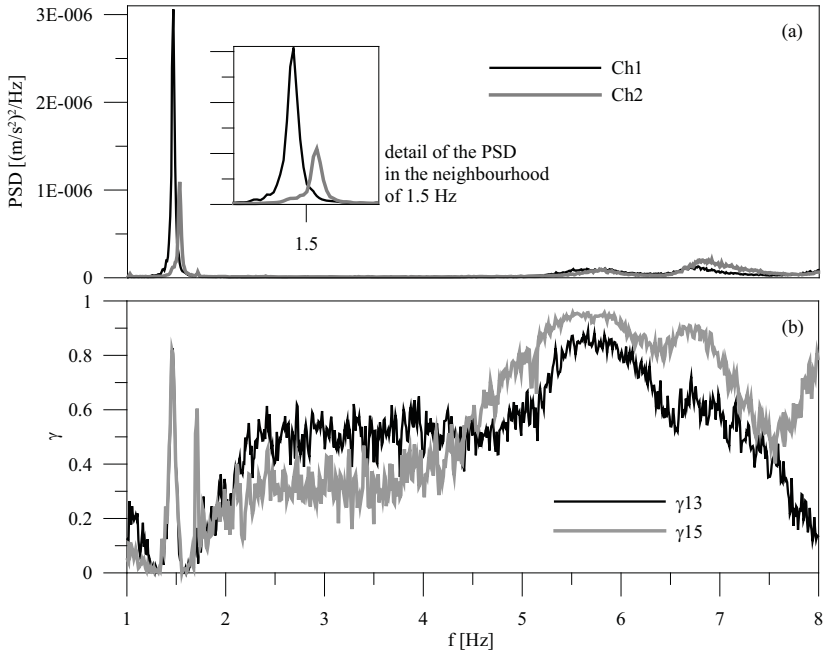

Fig. 2. Power Spectral Densities of accelerations measured on the top of the column (a) and coherence function among channel 1 and channels 3 and 5(b).

As a first step, the power spectral densities of the accelerations are observed. Figure 2a reports the PSDs of the two measurement points on the top of the column, in the frequency band where natural frequencies are expected. Two peaks in the neighborhood of 1.5 Hz emerge quite clearly (see details in Figure 2), while two other peaks appear in the range 5-8 Hz, but with strong damping. In such an unclear situation, the observation of the coherence (Figure 2 b) may be of some help. The coherence peaks are at the same frequencies as those observed

in the PSDs, suggesting that all these four peaks may in fact be representative of natural frequencies, as reported in Table 1.
Analogous results can be obtained from the singular value decomposition. Figure 3 reports the first singular value of the spectral matrix as a function of frequency, showing the two close peaks related to the first and second natural frequencies and the other peaks related to the third and fourth frequencies. The identified frequencies coincide with those detected with the peak picking, as reported in Table 1.

	f_1	f_2	f_3	f_4
PP, SVD	1.46	1.53	5.83	6.83
SSI	1.45	1.52	5.69	6.56
FE	3.14	3.32	15.68	17.52

Table 1. Experimental and numerical natural frequencies [Hz] of the Trajan column

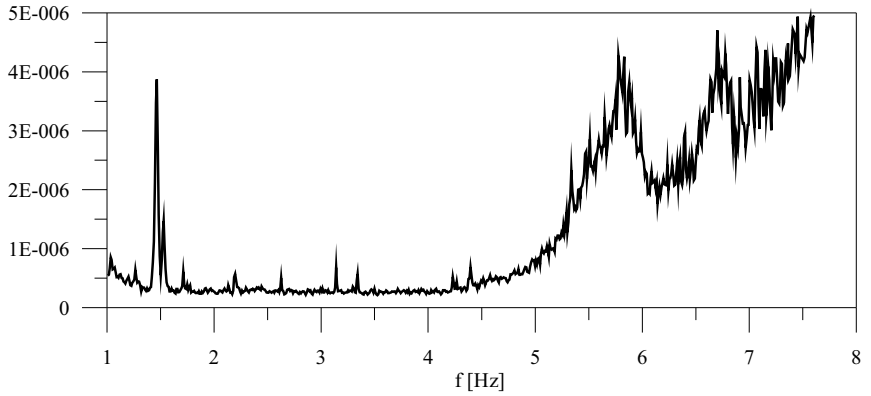

Fig. 3. First singular value of the spectral matrix as a function of frequency.

As a final step, the data are analyzed following the stochastic subspace decomposition. In this case, the evaluation of the model order is fundamental. A good model for modal analysis applications can be obtained by constructing stabilization diagrams, that is, by evaluating a set of models with different orders (Peeters, 2000). A criterion to state when an eigenvalue is stable must be defined; for instance, eigenvalues do not have to change more than 1% when the model order is increased. When an eigenvalue satisfies this stability criterion, its value is determined. Figure 4 shows the eigenvalue stabilization when increasing the model order and enables to define the natural frequencies that are reported in Table 1. The difficulties in the interpretation of the third and fourth frequencies, and related mode shapes, remain, in fact these frequencies stabilize for higher model order than the first and second. These difficulties, which concern in fact all the employed methods, are not surprising. In fact, the third and fourth frequencies are close to 6 Hz, which is the cutoff frequency of the ground, as was observed in other experimental tests on the Colosseum and Basilica of Maxentius (Pau & Vestroni, 2008; 2010). The ground attenuates frequencies which are smaller than 6 Hz and guarantees a white-noise spectrum in the frequency band 0-6 Hz. Therefore, for frequencies higher than 6 Hz, the hypotheses on the input, on which the present modal identification methods are based, are not satisfied.

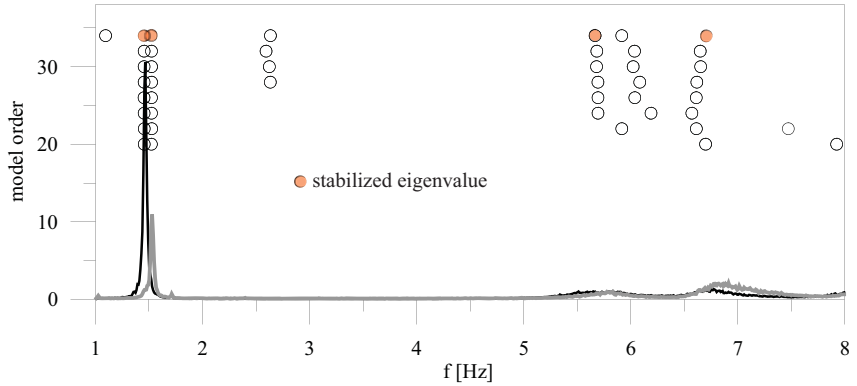

Fig. 4. Eigenvalue stabilization diagram for the Trajan column.

A comparison between the experimental mode shapes is now performed. The modal assurance criterion (MAC), which is a scalar product between the two mode shape vectors under consideration, normalized to the product of the moduli, is a measure of the agreement between two mode shapes. A comparison shows that the differences between the three techniques are very small for the first two modes (MAC$\simeq$ 0.99), but increase for the third and fourth modes (MAC $\simeq$ 0.8), which are identified with great difficulties in all the cases because of the strong damping. However, the results obtained by SVD and SSI agree each other better than those obtained by PP.

As regards the shapes of the modes, the mode shape pairs 1-3 and 2-4 strongly resemble those of a cantilever beam, as shown in Figure 5. For the sake of brevity, this Figure shows only the mode shapes determined by SSI method. Furthermore, the first two modes are nearly contained respectively into the two planes parallel to the base, while the third and fourth mode shapes are contained in planes which are not coincident with the measurement planes. This is also evident from Figure 2, as the peaks related to the first and second frequencies are present only in one of the two spectra, while the peaks related to the third and fourth are present in both the spectra. This experimental result was verified by a laboratory experiment on an axisymmetric clamped cylinder, a pipe with vertical axis, which was tested both in its nominally perfect and perturbed configuration. Figure 6 reports the projection onto the horizontal plane of the vertical planes containing the mode pairs 1-2, 3-4 and 5-6. Different colors relate to different test conditions. The tests show that even in nominally perfect conditions, the planes containing the mode shape pairs corresponding to the clamped beam can be different for each pair, especially for higher modes. Furthermore, each pair is contained in planes which only slightly deviate from orthogonality, consistent with the orthogonality of modes. These results can be ascribed to imperfections in geometry, which cause a deviation from perfect axisymmetry.

In conclusion, a comparison with the results provided by a numerical (FE) model is performed. The column is simply represented as a cantilever beam with varying section. In this model, the Young's modulus E and mass density ρ come from literature values determined by static tests on cores bored into the solid material. The natural frequencies obtained are reported in Table 1. These values are much higher than the experimental ones, and the reason is that the material parameters of the solid material are not representative of the behavior of the assembled system, where the interactions among the blocks have considerable

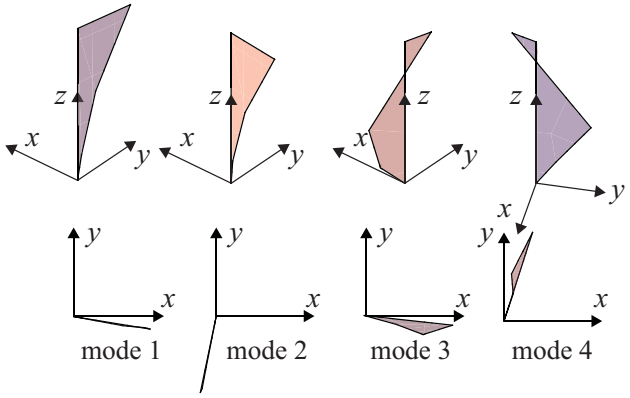

Fig. 5. Experimental mode shapes.

influence. A similar result was found by the authors in the analysis of the response of the Colosseum (Pau & Vestroni, 2008), where a reduction in the elastic modulus based on measurements of the wave propagation velocity in structural parts including joints brought the analytical and experimental results into satisfactory agreement. Here also, the reduction of the ratio E/ρ brings numerical and experimental results into satisfactory agreement. As regards the mode shapes, Table 2 shows that, whichever modal analysis method is used, the experimental modes 1 and 2 agree very well with the numerical ones. By contrast, for the pair 3-4 the mode shapes obtained by the SSI method have better quality.

	1	2	3	4
PP–FE	1.00	1.00	0.47	0.36
SVD–FE	0.98	0.95	0.62	0.55
SSI–FE	0.98	0.98	0.84	0.79

Table 2. MAC between experimental and numerical modes for the Trajan column

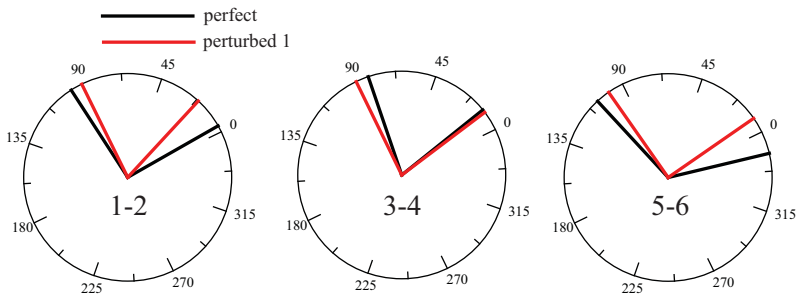

Fig. 6. Top view of the experimental mode shapes of a clamped pipe.

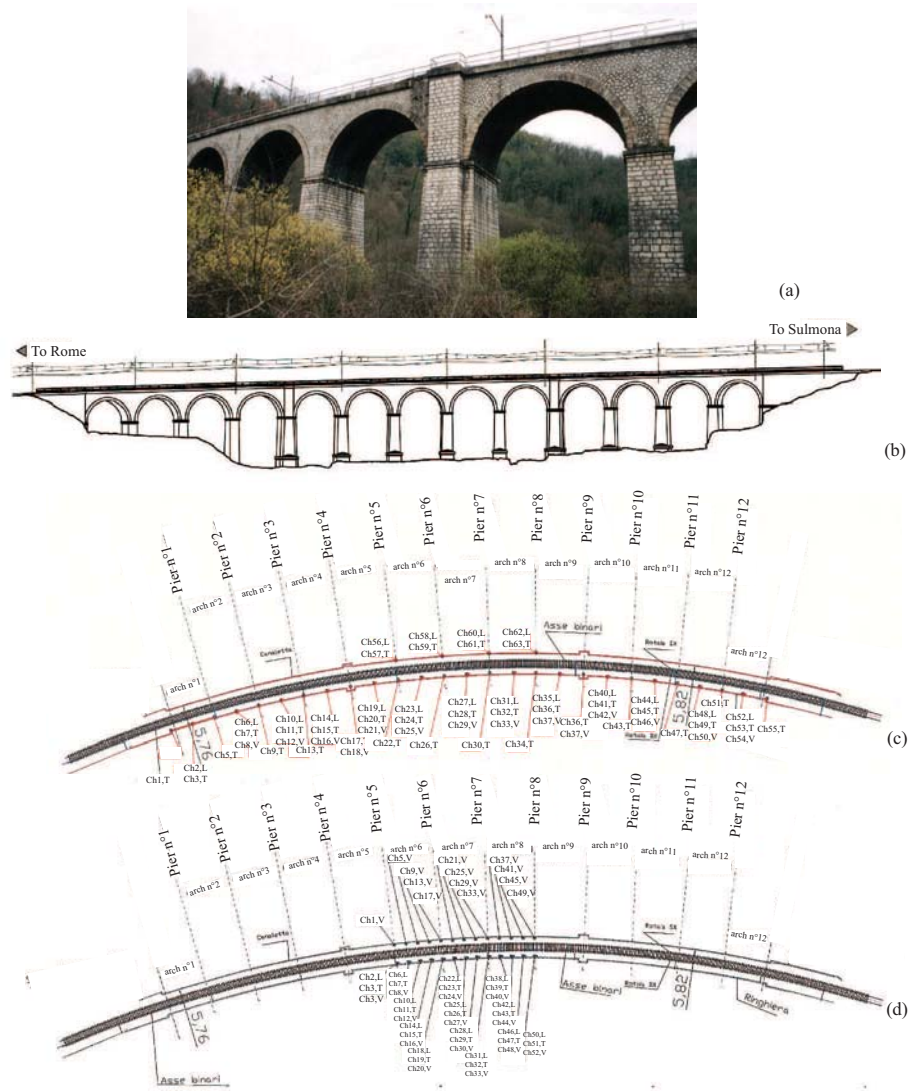

Fig. 7. Picture of the Vallone Scarpa bridge (a), front view (b) and plans (c,d) of the two accelerometer setups.

3.2 The Vallone Scarpa bridge

The Vallone Scarpa bridge was built at the end of the nineteenth century and is located along the Roma-Sulmona railway line, which crosses the central Italian region of Abruzzo. It is a masonry arch viaduct with thirteen bays, each with a span of 10 m. The piers are about 9 m in height (Figure 7). The plan has a radius of curvature of 400 m; the slope of the line is 2.7 %. The ambient vibrations of the bridge were recorded using two different arrangements of accelerometers (Figure 7c,d) at a sampling frequency of $f_S = 120Hz$. The measurement

directions were: in the plan of the deck, tangent to the bridge axis (L, longitudinal) and related orthogonal line (T, transverse), and the vertical direction (V) along the viaduct axis. In the first setup (Figure 7c), transverse sensors were placed on top of each pier, together with triaxial sets (T, L, V) located at the middle of each span. In the second setup (Figure 7d), triaxial sets of accelerometers (L,T,V) were placed on the deck edges of the three central bays.
To start with, the PSDs are examined. Figure 8(a) shows the PSDs measured at channels 19-21 of the first arrangement of sensors, placed on the fifth bay of the bridge. This figure immediately points out that, in this frequency range, the vertical and longitudinal components of the modes are much smaller than the transverse ones. These PSDs, at a glance, also enable to detect some peaks that are representative of the first natural frequencies of the structure. However, the identification of their values is very difficult because of the closeness of frequencies and strong damping, as is often the case with masonry structures. For instance, two very close peaks are present in the neighborhood of 3.9 Hz. The coherence function, which is shown in Figure 8(b), also shows peaks in correspondence with the peaks of PSDs, but does not help in resolving the close resonances.

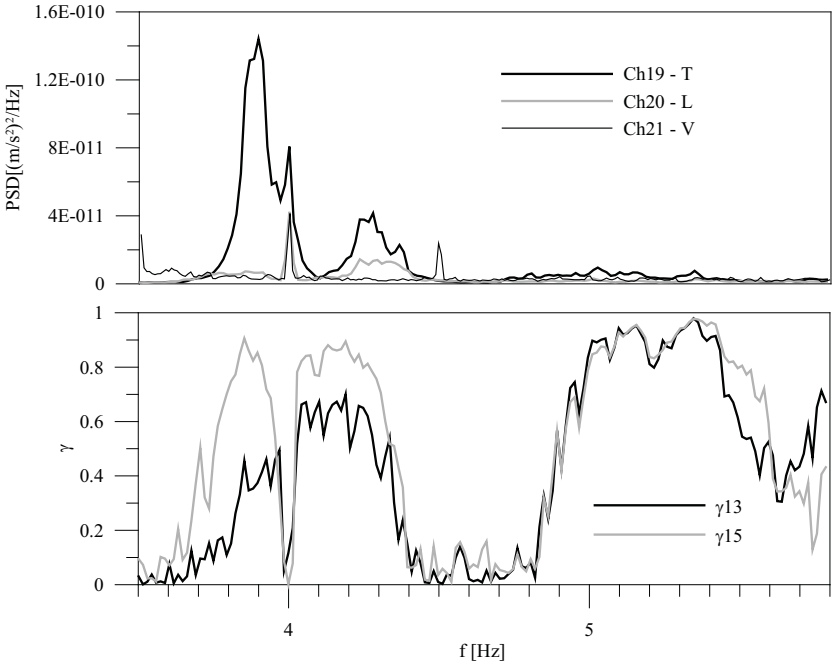

Fig. 8. PSDs (a) and coherence (b) of the accelerations measured on the fifth bay of the Vallone Scarpa bridge.

The technique of singular value decomposition points out analogous difficulties, as can be seen from Figure 9, that reports the first singular value of the spectral matrix for both setups as a function of frequency. An advantage of this technique compared to peak picking is the easier and faster determination of mode shapes, which enables to choose the peaks representative of natural frequencies.
Using the SVD with the first arrangement of sensors, the first five frequencies listed in Table 3 were determined. The stabilization diagram shown in Figure 10 furnishes frequencies,

obtained using SSI, similar to those obtained from SVD and PP (Table 3). Figure 10 also shows that a high model order is necessary to detect natural frequencies, which is computationally very much demanding, especially when using such a large number of accelerometers.
The mode shapes are bending modes of a beam over elastic supports in the plane of the deck, as shown in Figure 11, which depicts the first five modes of the structure. As for frequencies, SVD and SSI provide similar mode shapes. The main component of the mode shape is also in the transverse direction, as shown in Figure 11, which reports a comparison between the longitudinal and transverse components of each mode.

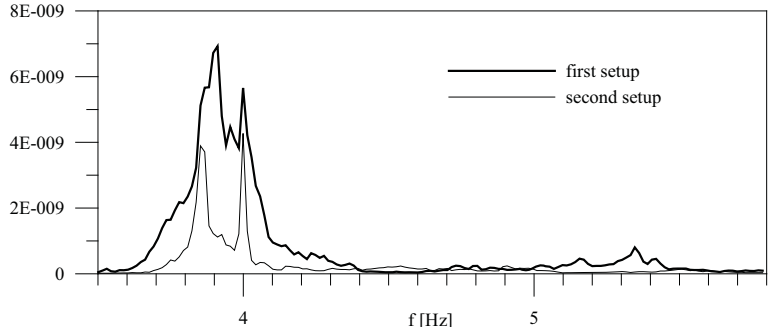

Fig. 9. First singular value of the spectral matrix as a function of frequency.

	f_1	f_2	f_3	f_4	f_5
PP, SVD	3.87	3.88	4.24	4.73	5.49
SSI	3.82	3.98	4.57	4.74	5.33
FE	2.41	2.71	2.92	3.44	3.76

Table 3. Experimental and numerical natural frequencies [Hz] of the Vallone Scarpa bridge

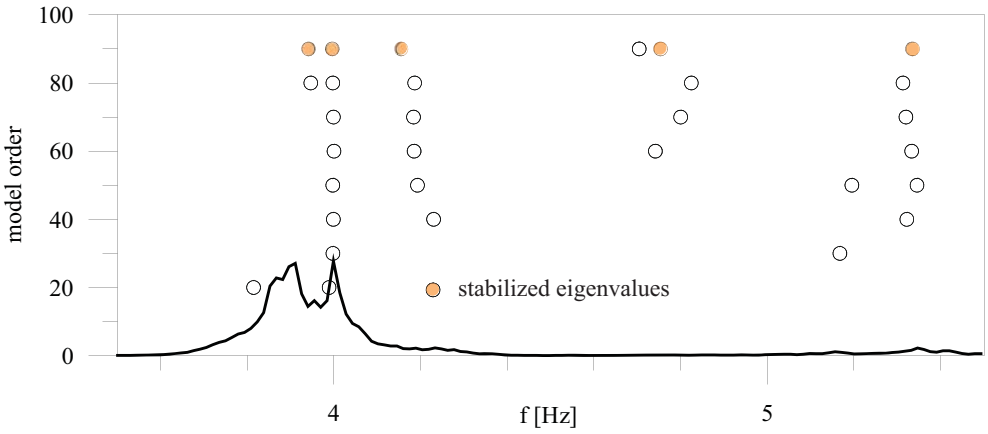

Fig. 10. Eigenvalue stabilization diagram for the Vallone Scarpa bridge.

The measurements performed with the second arrangement of sensors provided similar results, but showed in addition that the identified modes presented a slight rotational

component, shown by the opposite sign of the modal displacements measured on the right and left edges of the deck. This is shown in Figure 12, only for modes 3 and 4 for brevity. Furthermore, in the second arrangement of sensors there was a slight variation of frequencies, with an inversion between the order of modes 1 and 2. According to these measurements, the first mode presents one node, while the second one does not have any. This phenomenon is related to the closeness between the two frequencies of the arch in the horizontal plane and to the possible slight variation of the mechanical parameters between a measurement set and the other. A complete explanation of the phenomenon would require a repetition of the measurements and a verification of their robustness with regard to the ambient conditions.

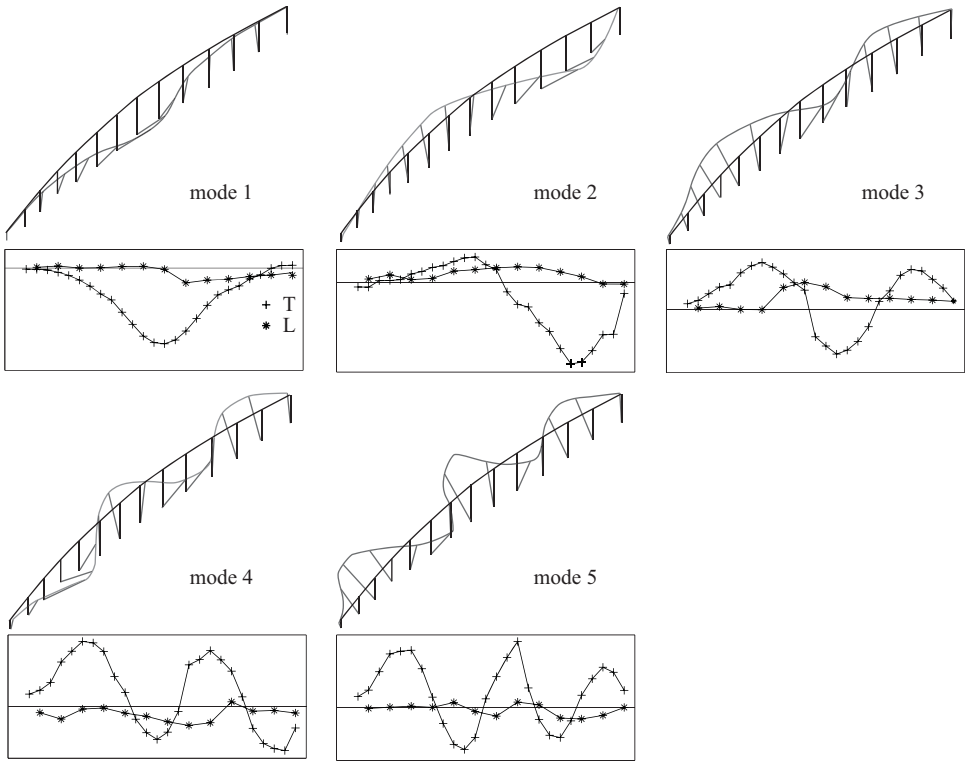

Fig. 11. Mode shapes of the Vallone Scarpa bridge and comparison between longitudinal (crosses) and transverse components (asterisks).

A finite element model of the bridge was also built to perform a modal analysis. The natural frequencies obtained are reported in Table 3 and are lower than those experimentally detected. The observed differences may be considerably reduced with a magnification of the mechanical parameters. In fact, the required updating is opposite in sign and smaller than that needed for the Trajan column. This depends on the fact that in a brick masonry the mechanical behavior of a specimen is much more representative of the behavior of the continuum than in the case of a dry block masonry. Analogous results were observed by the authors in (Pau & Vestroni, 2010). A comparison between experimental and numerical mode shapes, reported in Figure 13, presents a good agreement.

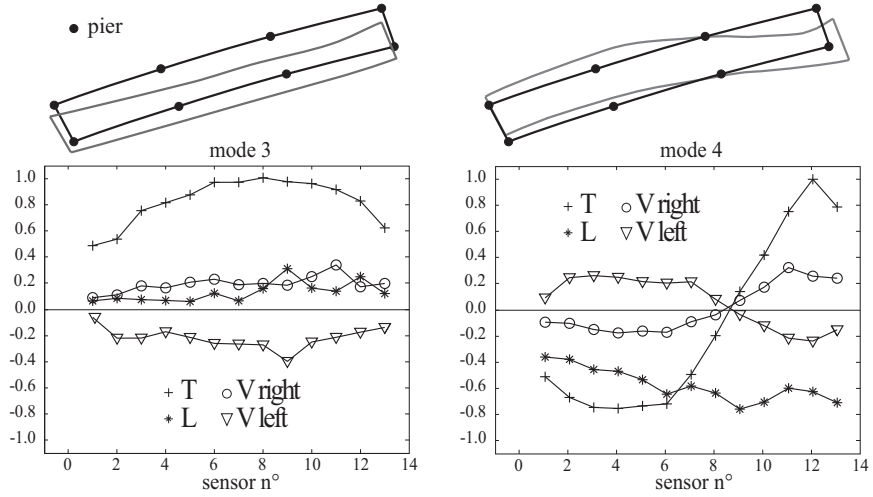

Fig. 12. Comparison between longitudinal, transverse and vertical components of experimental modes 3 and 4.

4. Conclusions

The ambient vibration response of two masonry structures, the Trajan column and the Vallone Scarpa bridge, has been analyzed using three widespread techniques, namely, the peak picking, singular value decomposition and stochastic subspace identification. The two structures are very different in masonry typology, with large blocks connected by clamps and pins for the Trajan column and mixed brick masonry for the Vallone Scarpa bridge. Notwithstanding the low level of excitation, the analysis has shown that the first frequencies of the structures are quite easily detectable. However, when higher frequencies are sought, difficulties may arise due to the lack in the verification of the hypothesis requiring that the input is white noise. Among the three different techniques considered, the SSI is the most demanding from a computational point of view and in general provides a better quality for mode shapes. As regards the comparison with finite element models, it has been shown that after an updating of the material properties of the finite element models, an agreement between experimental and numerical frequencies can be obtained. When dealing with dry masonry structures, this updating can imply a strong reduction of the Young's modulus since the material parameters of the solid material are not representative of the assembly, where the interactions between the blocks have considerable influence. In other types of masonry, such as the brick type, the behavior of a specimen is more representative of the continuum from which it is extracted and the required updating is more limited.

5. Acknowledgements

The authors wish to thank the RFI, Rete Ferroviaria Italiana company, which provided funds for the tests conducted on the Vallone Scarpa Bridge and in particular Dr. Giacomo Kajon, from the Experimental Institute of Italian National Railways, who was responsible for the experimental activities. The experimental tests on the Trajan Column were performed by the personnel of the Laboratory of the Department of Structural and Geotechnical Engineering of La Sapienza University of Rome with the consent of the Roman Soprintendenza Archeologica.

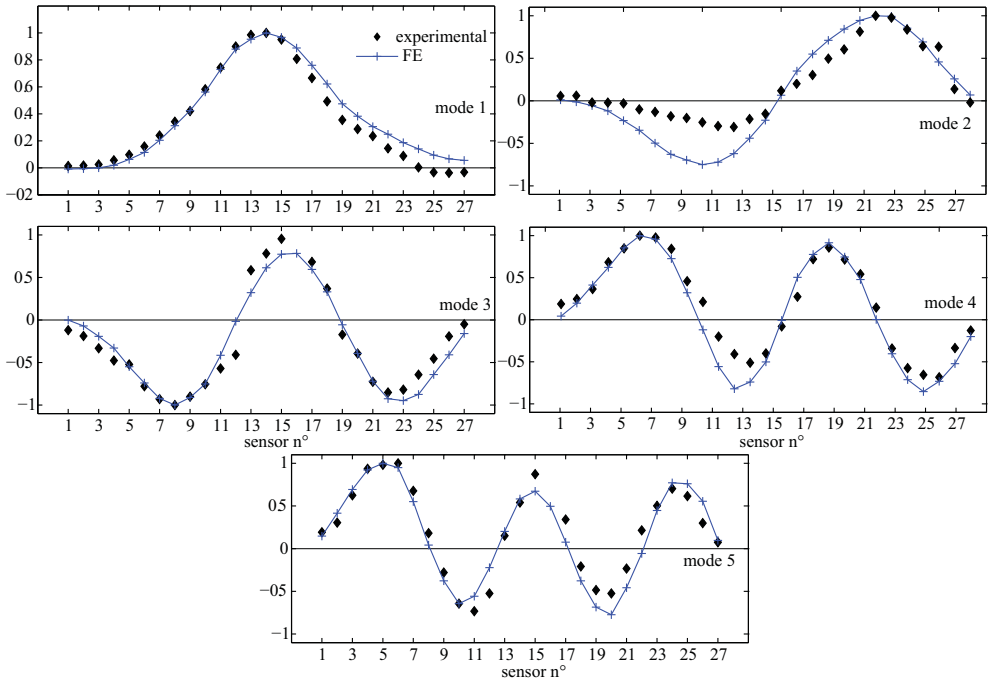

Fig. 13. Comparison between numerical and experimental transverse components of the mode shapes of the Vallone Scarpa Bridge.

6. References

Bendat, J. S. & Piersol, A. G. (1980). *Engineering applications of correlation and spectral analysis*, Wiley, New York.

Brincker, R., Zhang, L. & Andersen, P. (2001). Modal identification of output-only systems using frequency domain decomposition, *Smart Materials and Structures* Vol. 10: 441–445.

Brownjohn, J. M. W. (2003). Ambient vibration studies for system identification of tall buildings, *Earthquake engineering and structural dynamics* Vol. 31(No. 1): 71–95.

De Sortis, A., Antonacci, E. & Vestroni, F. (2005). Dynamic identification of a masonry building using forced vibration tests, *Engineering Structures* Vol. 0(No. 27): 155–165.

Ewins, D. J. (2000). *Modal testing: Theory and practice*, Research Studies Press Ltd., Hertfordshire, U.K.

Farrar, C. R., Doebling, S. W. & Nix, D. A. (2001). Vibration-based structural damage identification, *Philosophical Transactions of the Royal Society of London A* Vol. 359: 131–149.

Friswell, M. I. & Mottershead, J. E. (1995). *Finite element model updating in structural dynamics*, Kluwer Academic, Dordrecht, The Netherlands.

Gentile, C. & Saisi, A. (2007). Ambient vibration testing of historic masonry towers for structural identification and damage assessment, *Construction and building materials* Vol. 21: 1311–1321.

Juang, J. N. (1994). *Applied system identification*, Prentice-Hall, Englewood Cliffs, N.J.

Maia, N. M. M. & Silva, J. M. M. e. (1997). *Theoretical and experimental modal analysis*, Research Studies Press Ltd., Hertfordshire, U.K.

Morassi, A. & Vestroni, F. (2009). *Dynamic Methods for Damage Detection in Structures*, Springer.

Pau, A. & Vestroni, F. (2008). Vibration analysis and dynamic charachterization of the colosseum, *Structural Control and Health Monitoring* Vol. 15: 1105–1121.

Pau, A. & Vestroni, F. (2010). Dynamic characterization of the basilica of maxentius in rome, *Proceedings of the Int. Conf. on Noise and Vibration Engineering ISMA*, Leuven, Belgium.

Peeters, B. (2000). *System identification an damage detection in civil engineering*, PhD thesis, Katholieke Universitaet Leuven.

Ren, W. X., Zhao, T. & Harik, I. E. (2004). Experimental and analytical modal analysis of steel arch bridge, *Journal of Structural Engineering* Vol. 7(No. 130): 1022–1031.

Van Overschee, P. & De Moor, B. (1993). Subspace algorithms for the stochastic identification problem, *Automatica* Vol. 29(No. 3): 649–660.

Van Overschee, P. & De Moor, B. (1994). N4sid: Subspace algorithms for the identification of combined deterministic-stochastic systems, *Automatica* Vol. 30(No. 1): 75–93.

Van Overschee, P. & De Moor, B. (1996). *Subspace Identification for Linear Systems, Theory, Implementation, Applications*, Kluwer Academic Publishers, Boston.

Vestroni, F. & Capecchi, D. (1996). Damage evaluation in cracked vibrating beams using experimental frequencies and finite element models, *Journal of Vibration and Control* Vol. 2: 269–286.